AUTOMATIC IVUS MEDIA-ADVENTITIA BORDER EXTRACTION USING DOUBLE INTERFACE GRAPH CUT SEGMENTATION

Ehab Essa, Xianghua Xie

Department of Computer Science
Swansea University, UK

Igor Sazonov, Perumal Nithiarasu

College of Engineering
Swansea University, UK

ABSTRACT

We present a fully automatic segmentation method to extract media-adventitia border in IVUS images. Segmentation in IVUS has shown to be an intricate process due to relatively low contrast and various forms of interferences and artifacts caused by, for example, calcification and acoustic shadow. Graph cut based methods often require careful manual initialization and produces in consistent tracing of the border. We use a double interface automatic graph cut technique to prevent the extraction of media-adventitia border from being distracted by those image features. Novel cost functions are derived from using a combination of complementary texture features. Comparative studies on manual labeled data show promising performance of the proposed method.

Index Terms— IVUS, media-adventitia border, graph cut, optimal interface segmentation

1. INTRODUCTION

Intra-vascular Ultrasound (IVUS) imaging is a valuable complementary modality to angiography in coronary disease diagnosis and treatment. It is the modality that has been widely used for clinicians to assess the severity of a lesion, perform plaque classification, and determine the location and size for stenting. It is a catheter-based technology, which shows two-dimensional cross-sectional images of the coronary structure. A typical IVUS B-mode image consists of three regions: the lumen, the vessel that includes the intima and media layers, and the adventitia around the vessel wall. Among many other techniques, formulating the IVUS segmentation as a cost function minimization problem has been a popular approach. In [1], dynamic programming is used to search a minimum path in the cost function, which incorporates edge information with a simplistic prior, based on echo pattern and border thickness. Manual initialization is necessary. In [2], the border detection is carried out on the envelope data before the scan conversion. The authors applied spatio-temporal filters to highlight the lumen, based on the assumption that the blood speckles have higher spatial and temporal variations than arterial wall, followed by a graph-searching method similar to [1]. However, image features introduced by acoustic shadow or metallic stent would seriously undermine the assumption. Catheter movement can also cause spatial and temporal fluctuation, which leads to ambiguities. The *s-t* cut method [3] is employed in [4] to segment 3D IVUS data. Vertical intensity pattern along the borders, Rayleigh distribution and Chan-Vese minimum variance criterion are used in designing the cost functions. This intensity based features are susceptible to image variations that commonly exist in IVUS, such as calcification and shadow.

In this work, our focus is on automatically extracting media-adventitia border, i.e. outer vessel wall, which can be combined with lumen extraction from angiogram that only provides inner vessel wall. To tackle the intensity inhomogeneity and those interferences caused by undesired images features, global shape priors, such as using active appearance model [5], may be used. However, this approach requires consistency between training data and testing images, which is not trivial to achieve. For example, patients with more calcification or plaque can show large differences in acoustic appearance. Also, the geometrical shape can vary significantly from patient to patient, particularly for disease cases. Here, we use a bottom-up data driven approach. However, in order to achieve reliable results automatically, we apply double-interface graph cut segmentation. Those impediments, such as stent or soft and fibrotic plaque, appear inside media-adventitia border, and the acoustic signal decays rapidly in the adventitia so that there is largely no strong features beyond the media-adventitia border. This observation inspired us to apply an additional interface searching inside the media-adventitia border which links those undesired image features, including partial lumen border, and hence preserves the border of interest. A combination of complementary texture features is used, instead of image intensity, to form the basis of the boundary based cost functions.

2. PROPOSED METHOD

Briefly, the IVUS images are first transformed from Cartesian coordinates to polar coordinates. A node-weighed directed graph is then constructed so that the border extraction is considered as computing a minimum closed set. The search for this minimum closed set is solved by computing a minimum *s-t* cut in a derived arc-weighted directed graph. For our double-interface segmentation, an additional set of arcs

is constructed, taking into account the topological interrelation between the two interfaces. The associated cost functions are based on image features extracted using first derivative of Gaussian, Gabor filters and local phase transform. Finally, the extracted media adventitia border is smoothed using radial basis function (RBF) interpolation.

2.1. Preprocessing

The preprocessing is to transform the IVUS images from Cartesian coordinates to polar coordinates and to remove catheter region from the transformed images. Representing the images in polar coordinates is important to facilitate feature extraction in terms of radial and tangential characteristics. It also facilitates the automated graph cut in searching for minimum closed sets, where an open-ended height field is preferred. Moreover, the post-processing can then be carried out more efficiently since it becomes a one dimensional interpolation instead of two-dimensional.

2.2. Graph construction

Conventional graph cut, such as [3], generally requires user initialization, and more importantly only deals with one interface, i.e. foreground and background separation. Alternative methods, such as active contour and level set techniques, e.g. [6], can track multiple interfaces. However, they often require user initialization and do not guarantee a global minimum. Furthermore, since one of our interfaces is attracted by image features, such as calcification, which varies from image to image, it does not have consistent shape characteristics. Hence, deformable model with multiple interfaces, such as [7], may not be suitable.

In [8], the authors proposed a novel graph construction method, which transforms the surface segmentation in 3D into computing a minimum closed set in a directed graph. We adapt this method to a 2D segmentation, which can carry out double-interface segmentation simultaneously in low order polynomial time complexity and does not require user initialization. This approach also allows us to impose topological constraint, i.e. the two interfaces in our case can not intersect or overlap and the media-adventitia border is the outer interface (or lower interface when the IVUS image is transformed to polar coordinates).

For each desired interface, construct a graph $G = \langle V, E \rangle$, where each node $V(x, y)$ corresponds to a pixel in 2D image $I(x, y)$. The graph G consists of two arc types: intra-column arcs and inter-column arcs. For intra-column, along each column, every node $V(x, y)$ where $y > 0$ has a directed arc to the node $V(x, y - 1)$. In the case of inter-column, for each node $V(x, y)$ a directed arc is established to link with node $V(x + 1, max(0, y - \Delta))$, where Δ controls the smoothness of the interface. Similarly, node $V(x + 1, y)$ is connected to $V(x, max(0, y - \Delta))$. The last row of the graph is connected to each other to maintain a closed graph.

After constructing the graph for each of the two interfaces, taking into account interrelations between them is necessary and this is achieved by setting up another set of arcs to connect them. Geometrical and topological constraints can be imposed by setting minimum δ_{min} and maximum δ_{max} separation distances. The two interfaces thus will not intersect or overlap. This set of arcs, E^s, is defined as:

$$E^s = \begin{cases} \{V_1(x, y), V_2(x, y - \delta_{max}) | y \geq \delta_{max}\} \bigcup \\ \{V_2(x, y), V_1(x, y + \delta_{min}) | y < Y - \delta_{min}\} \bigcup \\ \{V_1(0, \delta_{min}), V_2(0, 0)\} \end{cases} \tag{1}$$

This graph construction requires the desired interfaces to be open-ended height fields, which in our case means that this will be carried out in polar coordinates.

2.3. Feature extraction

The media layer is usually very thin and generally dark in intensity, and the adventitia layer tends to be brighter, see Fig. 1 as an example. However, acoustic shadow, calcification, and other interfering image features are common. Hence, the feature extraction is concerned with enhancing the difference between media and adventitia and suppressing undesirable features.

First order derivative of Gaussian - This set of filters is designed to highlight the intensity difference between media and adventitia. Four different orientations are used.

Band-pass log-Gabor - Log Gabor is used as a bandpass filter in three scales to enhance the border and to reduce speckles and other image artifacts. To minimize possible overlap with the derivative of Gaussian filter in extracting edge features, this process is carried out in coarser scales, i.e. in the 3rd, 4th and 5th scales. Hence, these features particularly show dominant edges.

Local phase symmetric and asymmetric features - Local phase [9] employs spatio-temporal technique to enhance edge and bar-like features and suppress speckles in ultrasound images. Features like edges exist in the Fourier components at maxima in phase congruency [9], which can be located at peaks in the local energy function obtained by convolving odd $o_m(x, y)$ and even $e_m(x, y)$ symmetric Log Gabor filter to remove DC component and preserve phase in localized frequency. Two types of features can be extracted from phase congruency: feature asymmetry $FA(x, y)$ and feature symmetry $FS(x, y)$. Feature asymmetry highlights step-like image patterns, and is defined as:

$$FA(x, y) = \sum_m \frac{\lfloor [|o_m(x, y)| - |e_m(x, y)|] - T_m \rfloor}{A_m(x, y) + \varepsilon} \tag{2}$$

where m denotes filter orientation, ε is a small constant, T_m is an orientation-dependent noise threshold, $A_m(x, y) = \sqrt{e_m^2(x, y) + o_m^2(x, y)}$ and $\lfloor . \rfloor$ denotes zeroing negative values. Feature symmetry favors bar-like image patterns, which is useful in extracting the thin media layer. Its dark polarity symmetry is used here [10]:

$$FS(x, y) = \sum_m \frac{\lfloor [-|e_m(x, y)| - |o_m(x, y)|] - T_m \rfloor}{A_m(x, y) + \varepsilon} \tag{3}$$

2.4. Cost function

Due to large variations in image features and the correlation between edge information and media-adventitia border, boundary based cost functions are used. The cost function indicates the likelihood of each node in the graph to belong to the minimum cost path that represents the desired interface. Two separate cost functions are used to capture the media-adventitia border and an auxiliary interface that is above media-adventitia, since these two interfaces have different characteristics in image feature and formation.

For the media-adventitia border, all the three types of features described in Sect. 2.3 are used. It takes the following form:

$$C_1(x,y) = C_d(x,y) + \alpha_1 C_G(x,y) + \alpha_2(1 - FS(x,y)) \quad (4)$$

where C_d denotes the term for derivative of Gaussian features, C_G is for log-Gabor, and α_1 and α_2 are constants. The derivatives of Gaussian responses from different orientations are summed together to form C_d. Similarly, C_G can be obtained by cascading the filtering responses across scales. In addition, more weight can be assigned to coarser scale features so that it presence the connectivity of media-adventitia border at the existence of acoustic shadow, e.g. $C_G = G^{(3)} + G^{(4)} + 1.5G^{(5)}$ as used here and $G^{(i)}$ denotes ith scale. Feature symmetry FS is useful in enhancing the thin layer of media. It is normalized beforehand, and since the middle of the layer has larger values $1 - FS$ is used in the cost function so that the interface between media and adventitia is highlighted. Note that each of the term in the cost function is normalized.

For the auxiliary interface that is above media-adventitia, we use a combination of log- Gabor feature and feature asymmetry:

$$C_2(x,y) = C_G(x,y) + \alpha_3(1 - FA(x,y)) \quad (5)$$

where α_3 is a constant. Since the derivative of Gaussian filter has relatively stronger response to local intensity variation, it is not included in this cost function. The combination of those two types of features leads the cost function to favor linking globally dominant image features, which very often is distractive for media-adventitia border segmentation.

2.5. Compute the minimum closed set

Each graph node is weighted by a value representing its rank to be selected in the minimum closed set graph where the arc costs between graph nodes are infinitive. The weight assignment is carried out according to:

$$w(x,y) = \begin{cases} C(x,y) & ify = 0, \\ C(x,y) - C(x,y-1) & otherwise. \end{cases} \quad (6)$$

where C denotes the cost function and w is the weight for each node in the directed graph, which serves as the base for dividing the nodes into nonnegative and negative sets. The *s-t* cut method can then be used to find the minimum closed set. The source s is connected to each negative node and every nonnegative node is connected to the sink t, both through a directed arc that carries the absolute value of the cost node itself. The two optimal interfaces correspond to the upper envelope of each minimum closed set graph. Solving this *s-t* cut problem provides us two interfaces in the polar-transformed IVUS images. The lower interface is the desired media-adventitia border.

2.6. Post-processing

The smoothing parameter in graph construction prevents sudden drastic changes in the extracted interfaces. However, the segmented media-adventitia may still contain local oscillations. Smoothing based post-processing can be adopted to eliminate such oscillations. Here, RBF interpolation using thin plate base function is used to effectively obtain the final interface. Note, due to the images have been transformed into polar coordinates, the RBF processing only needs to be carried out in 1D.

3. EXPERIMENTAL RESULTS

A total of 95 IVUS images from 4 acquisitions of 2 patients are used to evaluate the proposed method. These images contain various forms of soft and fibrous plaque, calcification, stent, and acoustic shadow. In most of the images, the blood speckle is so prominent that the lumen border is very difficult to see. For all the tested images, ground-truth via manual labeling is available for quantitative analysis. All the parameters are fixed: the minimum and maximum distance between two interfaces, δ_{min} and δ_{max}, are set to be 5 and 140 respectively, and cost function weightings are set as $\alpha_1 = 0.7$, $\alpha_2 = 0.5$, and $\alpha_3 = 0.5$.

The proposed method was compared against the *s-t* cut [3] and single-interface segmentation with the cost function in 4. The cost function for the media-adventitia was kept the same. The *s-t* cut method requires manual initialization, and its result is highly initialization dependent. Fig. 1 (a)-(b) show a typical result achieved using *s-t* cut. Even with reasonable care in initialization, the result was not satisfactory. The single-interface segmentation gave partial media-adventitia border, as shown in row (c). However, its performance degraded when there were interfering image structures. The proposed double-interface method achieved promising result even without any user interaction, see row (d). More comparative results are given in Fig. 2, which shows typical performance for each method. Table 1 provides the quantitative comparison between the single-interface approach and the proposed method. The proposed method achieved better accuracy and consistency. A qualitative comparison between manual labelling of the media-adventitia border and the proposed method is shown in Fig. 3.

4. CONCLUSION

We presented an automatic double-interface segmentation method, whose cost functions combine local and global image features and its geometric constrain is integrated in graph construction. An auxiliary interface is simultaneously

Table 1. comparison between single-interface and double-interface segmentation results. AD: area difference in percentage; AMD: absolute mean difference in pixel compared to ground-truth.

	Single interface		Double-interface	
	AD	AMD	AD	AMD
Mean	9.99	12.55	5.84	6.99
Std.	11.06	11.45	4.53	4.13
Min	1.60	1.76	1.47	1.75
Max	57.08	54.70	25.04	24.42

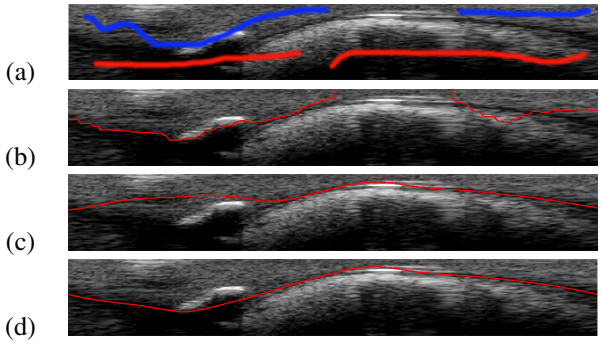

Fig. 1. (a): initialization for s-t cut, and its result shown in (b); (c): result by single interface segmentation; (d): proposed method.

searched to prevent undesirable image features from interfering the segmentation of media-adventitia border. Qualitative and quantitative comparison showed superior performance of the proposed method.

Acknowledgement - The authors would like to thank Dave Smith for supplying the medical data and NISCHR (WORD) for funding the project.

5. REFERENCES

[1] M. Sonka et al., "Segmentation of intravascular ultrasound images: A knowledge-based approach," in *T-MI*, 1995, vol. 14, pp. 719–732.

[2] A. Takagi et al., "Automated contour detection for high frequency intravascular ultrasound imaging: A technique with blood noise reduction for edge enhancement," in *Ultrasound Med. Biol.*, 2000, vol. 26, pp. 1033–1041.

[3] Y. Boykov and G. Funka-Lea, "Graph cuts and efficient n-d image segmentation," in *IJCV*, 2006, vol. 70, pp. 109–131.

[4] A. Wahle et al., "Plaque development, vessel curvature, and wall shear stress in coronary arteries assessed by x-ray angiography and intravascular ultrasound," in *Medical image analysis*, 2006, vol. 10, pp. 615–631.

[5] X. Chen et al., "3D automatic anatomy segmentation based on graph cut-oriented active appearance models," in *ICIP*, 2010, pp. 3653–3656.

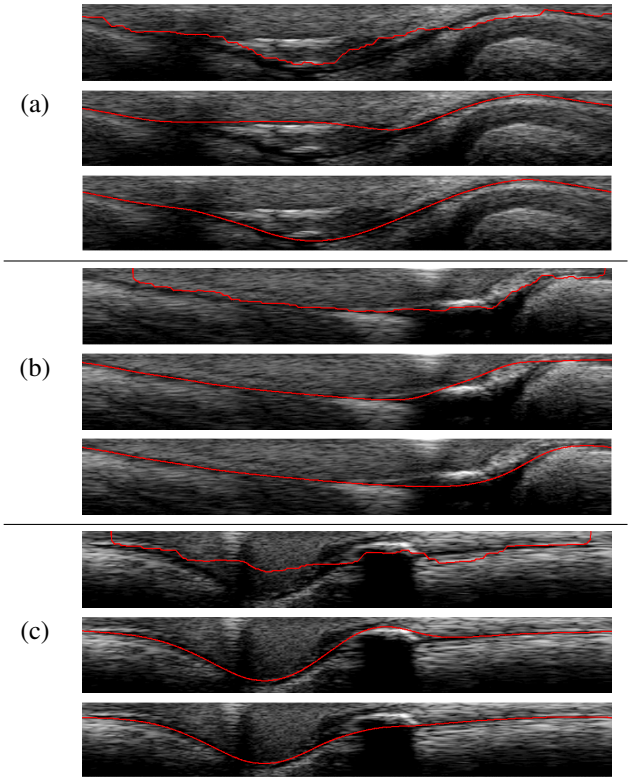

Fig. 2. Within each subfigure: first row shows the *s-t* result, second row shows single-interface result, and third row shows the proposed method.

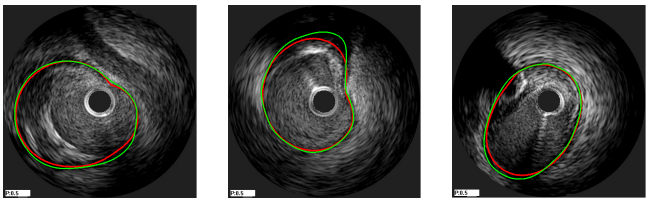

Fig. 3. Comparison between ground-truth (green) and the proposed method (red).

[6] L. Spreeuwers and M. Breeuwer, "Detection of left ventricular epi- and endocardial borders using coupled active contours," in *Computer Assisted Radiology and Surgery*, 2003, pp. 1147–1152.

[7] D. MacDonald, N. Kabani, D. Avis, and A. Evans, "Automated 3-D extraction of inner and outer surfaces of cerebral cortex from mri," in *NeuroImage*, 2000, vol. 12, pp. 340–356.

[8] K. Li et al., "Optimal surface segmentation in volumetric images-a graph-theoretic approach," in *T-PAMI*, 2006, vol. 28, pp. 119–134.

[9] M.Mulet-Parada and J.Noble, "2D + T acoustic boundary detection in echocardiography," in *Medical Image Analysis*, 2000, vol. 4, pp. 21–30.

[10] Peter Kovesi, "Symmetry and asymmetry from local phase," in *Tenth Australian Joint Conference on Artificial Intelligence*, 1997, pp. 185–190.